

## Effects of Magnetic Field on Corrosion Behaviour of X100 Pipeline Steel in Simulated Soil Solution Containing Sulphate-Reducing Bacteria

Gao Zhenbang <sup>1,2</sup>, Wang Dan <sup>1,2,\*</sup>, Jiang Jintao <sup>3</sup>, He Jianyu <sup>1,2</sup>, Wang Yue <sup>1,2</sup>, Xie Fei <sup>1,2,\*</sup>

<sup>1</sup> College of Petroleum Engineering, Liaoning Shihua University, Fushun 113001, China

<sup>2</sup> Key Laboratory of Oil and Gas Storage and Transportation Technology in Liaoning Province, Fushun 113001, China

<sup>3</sup> Liaohe Oilfield Oil and Gas Gathering and Transmission Company, Panjin, 124000, China

\*E-mail: [wd841015@163.com](mailto:wd841015@163.com) (Wang Dan); [xiefei0413@163.com](mailto:xiefei0413@163.com) (Xie Fei)

*Received:* 13 September 2021 / *Accepted:* 18 October 2021 / *Published:* 10 November 2021

---

The magnetic field (MF) is often utilized in engineering as a means of removing microbial bacteria. The effects of an MF on the electrochemical corrosion behaviour of X100 pipeline steel caused by sulphate-reducing bacteria (SRB) were investigated by electrochemical tests and scanning electron microscopy (SEM). The results showed that the MF inhibited the growth and activity of SRB, and the corrosion rate of X100 steel initially decreased and then increased with increasing MF strength. The lowest corrosion rate of X100 steel was observed under a 5-mT MF. These results are also attributed to the effect of the MF on the mass transfer of the corrosive medium..

---

**Keywords:** Magnetic field; Sulphate-reducing bacteria; X100 steel; Electrochemical corrosion; Mass transfer

### 1. INTRODUCTION

For safety and economic reasons, high-strength pipeline steel is the optimum choice for the efficient storage and transport of oil and gas. X100 pipeline steel is characterized by several economic advantages, including high strength, high pressure and low cost [1-3]. However, buried pipelines are often susceptible to corrosion risks. The corrosion of pipes in soils is a very complex process. In addition to the action of aggressive ions in the soil, microbiologically influenced corrosion (MIC) can cause severe corrosion damage [4-6]. In soil environments, approximately 20% of pipeline failures are associated with microbial activity, and sulphate-reducing bacteria (SRB) are involved in MIC [7, 8]. SRB typically adhere to metal surfaces and cause severe equipment failures and substantial economic losses [9-11]. Traditional microbial control involves the use of biocides, a considerable number of which

produce secondary contamination [12, 13]; thus, the development of improved methods for inhibiting bacterial growth is a current research topic.

Currently, the application of an MF to inhibit MIC has been widely studied [14-20]. The effect of an MF on the electrochemical corrosion of metallic materials can be described by magnetohydrodynamics (MHD), mainly in terms of the introduction of a Lorentz force into an electrolyte [21, 22]. The application of an MF over a specific range of intensities can inhibit corrosion. Most scholars consider that an MF inhibits MIC by inhibiting the growth of microorganisms and producing biofilms [23]. Liu et al. used electrochemical tests to investigate the effect of an MF on the corrosion behaviour of Q235 steel [13]. The MF inhibited the growth of iron oxide bacteria, reduced the formation of pits, and produced a dense biomineralized film on the steel surface. However, there is no consensus on the effect of an MF on MIC.

In this study, the effect of the MF strength on the microbial corrosion behaviour of X100 pipeline steel was investigated performing electrochemical tests and scanning electron microscopy (SEM) in a soil environment. The corrosion mechanism of X100 pipeline steel under MF was determined. The results of this study are useful for developing novel methods to control microbial corrosion of pipeline steel.

## 2. EXPERIMENTAL METHODS

### 2.1 Materials

The material used in the present study was API X100 pipeline steel, and its chemical composition (wt.%) is shown in Table 1. A uniform acicular ferrite structure containing inclusions accumulated at the grain boundaries is shown in Fig. 1.

**Table 1.** Chemical compositions of X100 pipeline steel (w.t.%).

C	Si	Mn	S	P	Al
0.05	0.25	1.83	0.002	0.08	0.02
Nb	Ni	Cu	Ti	Fe	
0.10	0.23	0.21	0.01	Bal	

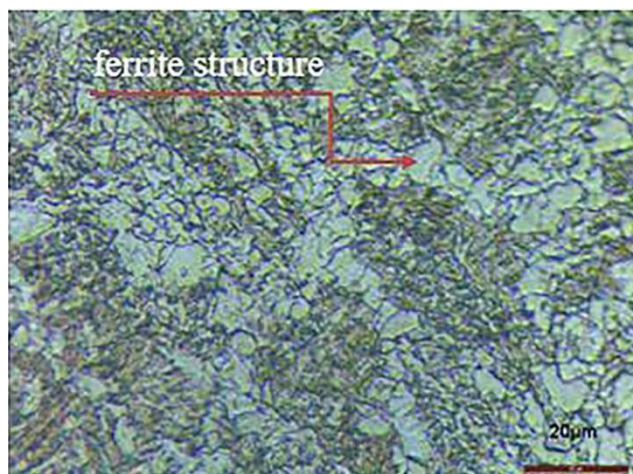


**Figure 1.** Microstructure of X100 steel

The material was cut into samples with dimensions of 50 mm × 25 mm × 2 mm and 10 mm × 10 mm × 2 mm. In the first type of sample, a 2-mm hole was drilled in the top to perform weight-loss experiments. The working area of the electrochemical sample was 1 cm<sup>2</sup>, and copper wires were attached by spot welding on the back of the sample. The nonworking surface was sealed with epoxy resin in a PVC tube for use in the electrochemical experiments. Before the experiments were performed, all the samples were sanded with SiC water sandpaper with grades ranging from #80 to #2000. Then, the samples were degreased with acetone and ethanol, cleaned and rinsed with deionized water, placed on a dry cold tray and subjected to UV disinfection 30 minutes before the experiment to eliminate bacterial interference.

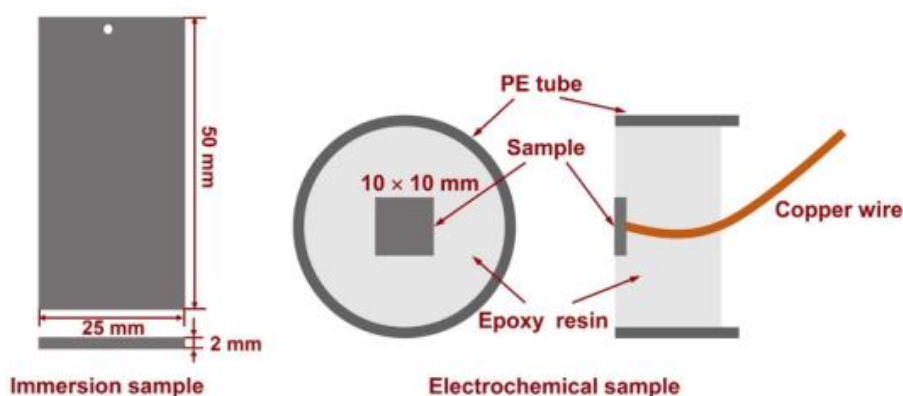


**Figure 2.** Schematic of the sample.

## 2.2 Test solution

A simulated soil solution was prepared from 0.1 mol/L NaCl, 0.1 mol/L NaHCO<sub>3</sub> and 0.1 mol/L Na<sub>2</sub>SO<sub>4</sub>, and the solution pH was adjusted to 7.4 with 5% NaOH. SRB strains were collected from the soil of Shenyang Soil Centre Station of the National Material Environment Corrosion Station and cultured in the SRB standard medium recommended by the American Petroleum Institute (API) [24].

Then, the medium was placed in an incubator ( $30 \pm 1$  °C) for 3-5 days. SRB strains were obtained after purification. The culture medium used in the experiment consisted of 0.5 g/L  $K_2HPO_4$ , 0.5 g/L  $Na_2SO_4$ , 1 g/L  $NH_4Cl$ , 0.1 g/L  $CaCl_2$ , 2 g/L  $MgSO_4 \cdot 7H_2O$ , 1 g/L yeast extract and 3.5 g/L sodium lactate. The pH of the medium was adjusted to  $pH 7.2 \pm 0.2$  with 5% NaOH. The experimental setup was disinfected and sterilized at 121.5 °C in a vertical-pressure steam sterilization pot for 15 min. The setup was allowed to cool, and 0.1 g/L ascorbic acid, 0.1 g/L sodium hydrosulphite and 0.1 g/L ammonium ferrous sulphate were added to the sterilized setup. The reagents used in the experiments were of analytical grade, and the media were all deionized. The medium was mixed with a sterilized soil simulant (1:1) to produce the experimental solution. Then, 6 mL of the SRB strain were inoculated into 300 mL of the test solution in a sterile control station.

Neodymium magnets (with different relative magnetic poles) were placed perpendicular to the ground and parallel to each other to serve as static MF devices. The MF direction was perpendicular to the sample surface, and galvanized white iron was used to create anti-interference isolation enclosures. The experimental apparatus is shown in Fig. 2. The MF strength was measured by an HT208 digital Tesla meter. Microbiological experiments were carried out using a UV-2550 UV spectrophotometer to measure the photometric value (optical density [OD]) of SRB. The OD of SRB in the simulated soil simulation was measured using a semicontinuous culture method under MF of 0, 2, 5, 7 and 10 mT. Growth curves under different MF strengths were drawn.

### 2.3 Electrochemical test

Weight-loss experiments were performed on five groups of samples, which were immersed in the simulated soil solution containing SRB by a static hanging method under MF intensities of 0, 2, 5, 7 and 10 mT; the samples were allowed to soak anaerobically in the solution for 14 days at 30 °C in a biochemical incubator. The surface morphologies of the samples were observed through scanning electron microscopy. The corrosion rates of the samples after 14 days of immersion in different MF strengths were calculated using the weightlessness method [Eq. (1)]. Three groups of parallel experiments were performed, and the reproducibility of the data was good.

$$v = \frac{\omega_1 - \omega_2}{S \times t} \quad (1)$$

In the formula presented above,  $v$  is the corrosion rate,  $g/m^2 \cdot h$ , and  $\omega_1$  and  $\omega_2$  are the quantities of the samples before and after immersion tests, respectively. After the immersion experiment was performed, the corrosion morphology of the samples was observed by scanning electron microscopy.

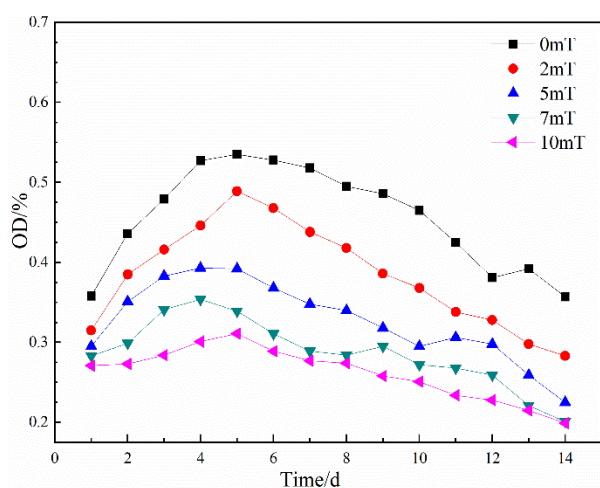
Electrochemical impedance spectroscopy (EIS) and potential polarization tests were performed on the electrochemical specimens. The electrochemical experiments were performed using a PARSTAT 2273 electrochemical workstation. A three-electrode system was used for the experiments. The working electrode was X100 steel, the auxiliary electrode was a platinum plate, and a saturated glyceryl electrode (SCE) was used as a reference electrode (unless stated otherwise, the potentials presented in this paper are relative to the SCE). The EIS was measured at a self-corrosive potential ( $E_{corr}$ ) with an excitation signal of 10 mV and a test frequency range of 100 kHz to 10 mHz. ZsimpWin software was used to analyse and process the AC impedance data. The potentiodynamic polarization curve was scanned at 0.5

mV/s, starting at -300 mV (vs. OCP) and ending at 0 V (vs. SCE).

### 3. EXPERIMENTAL RESULTS

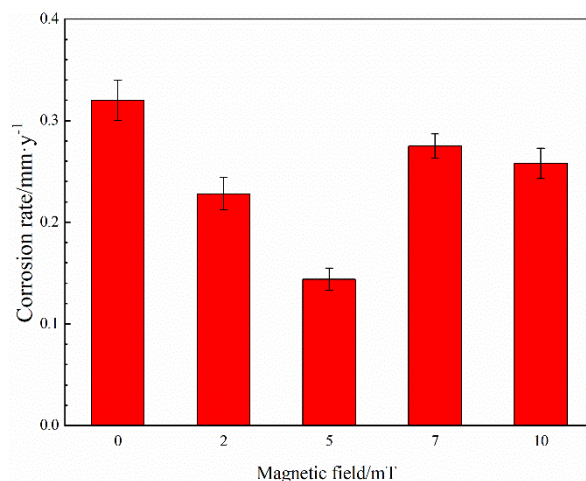
#### 3.1 Effect of magnetic field on SRB growth

The growth curves of SRB in the simulated soil solution under different MF strengths are shown in Fig. 3. As a result of semicontinuous culturing, the growth curves have a typical logarithmic phase, stable period and other characteristics. As the MF strength increases, the number of SRB decreases (Fig. 3), which indicates that the MF inhibits SRB growth. This result is consistent with previous findings [25, 26].



**Figure 3.** Growth curves of the SRB under different magnetic fields

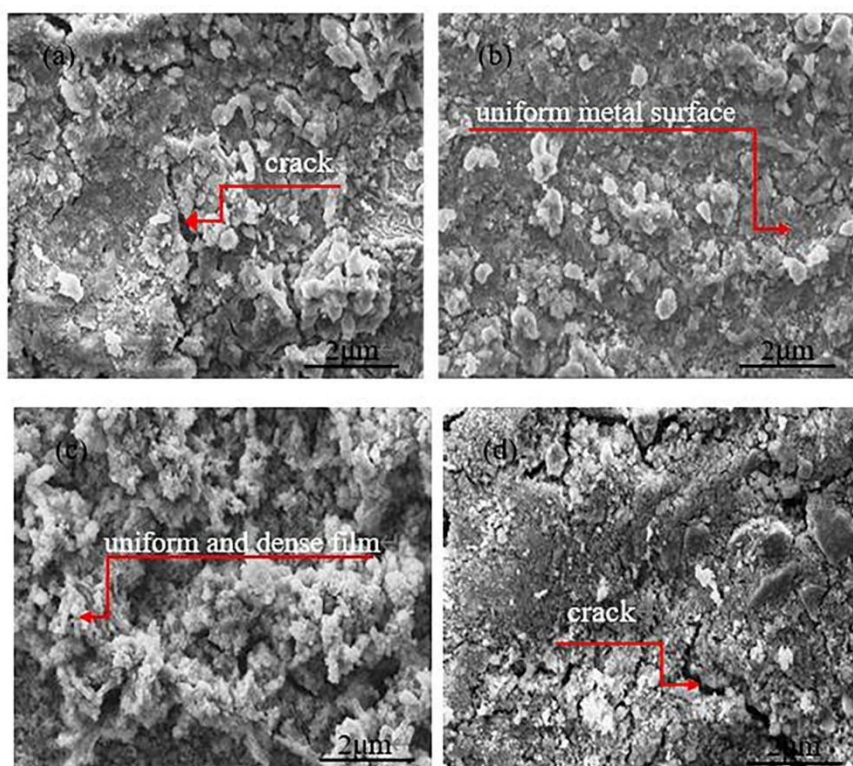
#### 3.2 Weight loss and surface corrosion morphology



**Figure 4.** Corrosion rate of the X100 steel under various magnetic field

The corrosion weight loss of X100 steel in the simulated soil solution containing SRB under different MF strengths decreases in the following order (Fig. 4): 0 mT > 10 mT > 7 mT > 2 mT > 5 mT. The results indicate that the external MF affects the corrosion rate. As the MF strength increases, the corrosion rate first decreases and then increases. The lowest corrosion rate is obtained for an MF strength of 5 mT, which is consistent with the results of Wang's study [15].

The morphology of the surface film layer of X100 steel that was soaked for 14 days in the simulated soil solution containing SRB under different MF strengths is shown in Fig. 5. In the absence of an MF, the X100 steel surface film is porous and contains cracks, and a local shedding phenomenon can be observed. A porous film creates a favorable environment for SRB growth and accelerate X100 steel corrosion. Under the application of an MF with a strength of 2 mT, the metal surface layer became uniform. Under application of a 5-mT MF, the surface film layer adsorbed on the steel surface was mostly uniform and dense. This phenomenon probably occurred because the surface layer of the main components of iron oxide and iron sulfide are easily magnetized materials, and the applied MF increased the uniformity and density of the surface layer. A mechanical barrier to the metal was thus created, thereby reducing the corrosion rate. Under application of a 7-mT MF, the film cracked again, showing that the physical-barrier effect of the film layer may have decreased. Under application of a 10-mT MF, local shedding phenomenon of the metal film became severe, and the corrosion rate gradually increased.



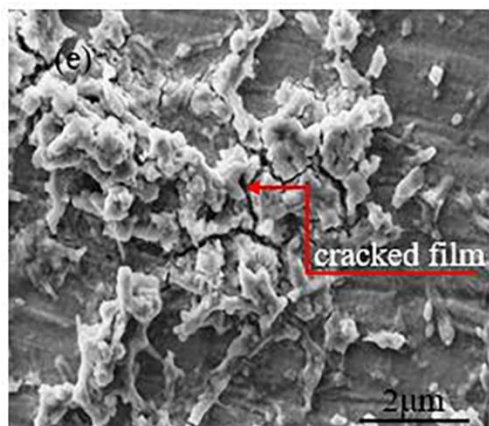


**Figure 5.** Surface morphology of X100 steel after immersion in simulated soil solution for 14 days under the various MF (a)0, (b)2, (c)5, (d)7 and(e)10 mT.

### 3.3 Polarization curve

The polarization curves of X100 steel under different MF strengths are shown in Fig. 6. With increasing MF strength, there is a small change in the slope of the cathodic polarization curve, whereas the anodic polarization curve slope changes significantly (Fig. 6). An increase in the MF strength from 0 mT to 5 mT shifts the polarization curve of the specimen to the left, the  $E_{\text{corr}}$  becomes more positive, and the corrosion current density decreases. An increase in the MF strength from 5 mT to 10 mT shifts the polarization curve to the right,  $E_{\text{corr}}$  becomes more negative, and the corrosion current density increases. The anodic region of the polarization curve exhibits an activation–inactivation transition region under different MF strengths. This result is similar to the polarization curve results obtained in a previous study [27].

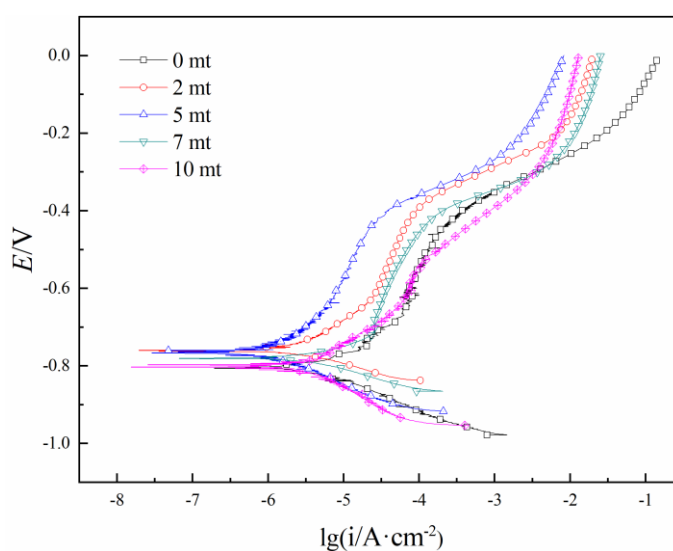


**Figure 6.** Potentiodynamic polarization curves of the X100 steel in the soil simulation solution containing SRB

Table 2 shows the results of fitting the polarization curves for X100 steel. As the MF intensity increases from 0 mT to 10 mT, the current densities are 8.52, 6.31, 3.16, 6.83 and 7.34  $\mu\text{A}/\text{cm}^2$ . As the MF strength increases from 0 mT to 5 mT, the corrosion current density of X100 steel decreases gradually, and the smallest corrosion rate is obtained (5 mT). As the MF strength increases to 10 mT, the corrosion current density increases again. The applied MF inhibits the corrosion rate of X100 steel in the simulated soil solution containing SRB, where the inhibitory effect first increases and then decreases with increasing MF strength. When the MF strength reaches 5 mT, the degree of inhibition is maximized and the smallest corrosion rate is obtained. When the MF strength exceeds 5 mT, the corrosion rate of X100 steel increases gradually. Considering Fig. 3 presented above shows that as the MF strength increases, the number of SRB gradually decreases, that is, the MF inhibits the growth of SRB. This result further illustrates that the MF affects microbial corrosion of X100 steel by inhibiting SRB growth.

**Table 2.** Polarization curve parameters at different MF strength parameters

Condition	$E_{\text{corr}}(\text{V})$	$I_{\text{corr}}(\mu\text{A}/\text{cm}^2)$	$b_a$	$b_c$
0 mT	-0.81	8.52	0.202	-0.267
2 mT	-0.76	6.31	0.216	-0.254
5 mT	-0.74	3.16	0.193	-0.246
7 mT	-0.79	6.83	0.207	-0.251
10 mT	-0.81	7.34	0.221	-0.246

### 3.4 Influence of magnetic field on EIS

Fig. 7 shows the EIS results for X100 steel under different MF conditions. The Nyquist diagram shows that the impedance spectrum exhibits capacitive arc characteristics. As the MF intensity increases from 0 mT to 10 mT, the diameter of the capacitive arc increases and then decreases. The corrosion resistance of the samples can be arranged in descending order in terms of the MF strength as follows: 5 mT > 2 mT > 7 mT > 10 mT > 0 mT. This finding is consistent with the polarization curve analysis. There are two-time constants in the corresponding Bode diagram for X100 steel under different MF strengths.

The Nyquist plots were fitted using the equivalent circuit presented in Fig. 8, and the fitting results are shown in Table 3. In the equivalent circuit diagram,  $C_f$  is the equivalent microbial film and corrosion product film capacitance;  $C_{dl}$  is the electric double-layer capacitance of the electrode;  $R_s$  is the electrolyte solution resistance between the working and reference electrodes;  $R_f$  is the resistance of the corrosion product film;  $R_t$  is the charge-transfer resistance for the electrode reaction; and  $R_p$  is the polarization resistance, where  $R_p = R_t + R_f$ .

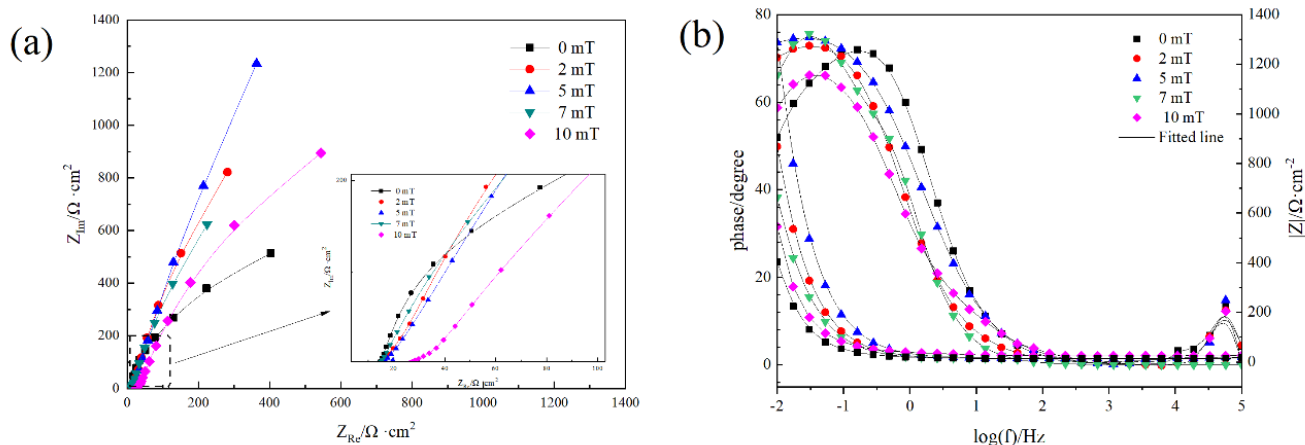


**Figure 7.** EIS of X100 steel under different magnetic fields

The larger the  $R_p$  is, the smaller the metal corrosion rate is.  $R_p$  initially increases and subsequently decreases with increasing MF strength. As the MF strength increases from 0 mT to 5 mT,  $R_p$  gradually increases. The largest  $R_p$  is achieved at an MF strength of 5 mT. As the MF strength increases from 5 mT to 10 mT,  $R_p$  gradually decreases.  $R_f$  and  $R_t$  increase as the MF strength increases from 0 mT to 5 mT.  $R_f$  and  $R_t$  decrease as the MF strength increases from 5 mT to 10 mT.

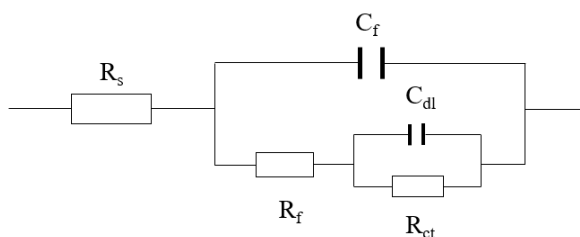


**Figure 8.** Equivalent circuit diagram for the fitting of the impedance spectra

**Table 3.** EIS at different magnetic field strength parameters

Condition	$R_s/(\Omega \cdot \text{cm}^2)$	$C_{dl}/(\text{F} \cdot \text{cm}^{-2})$	$R_f/(\Omega \cdot \text{cm}^2)$	$C_f/(\text{F} \cdot \text{cm}^{-2})$	$R_p/(\Omega \cdot \text{cm}^2)$
0 mT	14.11	0.006171	1323	0.01368	45.2
2 mT	14.03	0.008342	2461	0.00749	56.58
5 mT	16.24	0.005416	4102	0.00518	125.8
7 mT	14.08	0.008709	1851	0.01258	85.4
10 mT	26.16	0.003349	1794	0.007841	50.23

#### 4. ANALYSIS AND DISCUSSION

Liu reported that the MF affects the corrosion rate of X100 steel in the SRB-containing simulated

soil solution in two ways, by affecting the SRB and the electrochemical reactions. As the MF increases, the number of SRB decreases, possibly because of the influence of the MF on the in vivo cytoplasmic or active proteins of SRB. The physiological characteristics of the proteins may be altered, thereby reducing the bacterial activity and number of bacterial cells. Under an MF with a strength of 0-5 mT, SRB exhibit increased activity and adhere to the steel surface to produce a dense biofilm (Fig. 5): the thick film layer prevents further corrosion, as shown by the increase in the film resistance and charge transfer resistance of the impedance spectrum (Table 3). Under an MF of 5-10 mT, the SRB activity is weak, and the biofilms on the steel surface crack, exposing the bare metal locally and leading to further corrosion, which manifests as a decrease in the film resistance and charge transfer resistance of the impedance spectrum.

The MF mainly affects electrochemical reactions by modifying the mass transfer in solution [28-31]. This effect can be understood in terms of MHD, that is, an MF produces a Lorentz force that affects the motion of a charge. That is, the Lorentz force causes a charge to move perpendicularly to the current and flux density and induces electrolyte convection, which in turn affects charge movement [32, 33]. As the X100 steel corrodes in the simulated soil solution containing SRB, numerous microscopic primary cells form on the steel surface. The micro battery reactions are as follows:



Based on the reactions presented above, the  $Fe^{2+}$  concentration near the surface of X100 steel is greater than that in the corrosive medium solution, and this concentration difference induces an upward natural convection. In addition, the application of an MF generates a Lorentz force on the ions, which induces a flow opposite to the direction of natural convection [34, 35]. Both flows create a troposphere. The corrosion rate of X100 steel in the SRB-containing simulated soil solution initially decreases and subsequently increases as the MF intensity increases. When the MF intensity is relatively small (2-5 mT), the upward flow caused by the force of the MF weakens natural convection. The surface troposphere of X100 steel gradually thickens, which protects the metal. Therefore, the corrosion rate of X100 steel is reduced. An MF of 5 mT produces the thickest troposphere and the smallest corrosion rate for X100 steel. As the MF strength increases (7-10 mT), the medium flow induced by the MF causes many  $SO_4^{2-}$  and  $Cl^-$  plasmas to reach the metal surface. These aggressive ions cause the corrosion rate of the metal surface to increase, and the  $Fe^{2+}$  concentration near the metal surface increases further. At this time, natural convection caused by the concentration difference predominates, the diffusion layer gradually thins, and the corrosion rate of X100 steel is gradually enhanced.

## 5. CONCLUSIONS

(1) As the MF intensity increased, the number of SRB decreased. This observation indicated that the MF inhibited SRB growth, where the degree of inhibition increased with the MF strength improved.

(2) Current densities were 8.52, 6.31, 3.16, 6.83 and 7.34  $\mu A/cm^2$  were obtained by increasing the MF strength from 0 mT to 10 mT. The lowest current density and degree of corrosion were obtained

at an MF intensity of 5 mT.

(3) The MF affected the microbial corrosion of X100 steel by inhibiting SRB growth and inducing flow of media flow.

#### ACKNOWLEDGEMENTS

This work was supported by Liaoning Provincial Scientific Research Project LJKZ0395.

#### References

1. K. Gong, M. Wu, G.X. Liu, *Corros. Sci.*, 165 (2020) 108382.
2. K. Gong, M. Wu, F. Xie, G.X. Liu, D.X. Sun, *Constr. Build Mater.*, 260 (2020) 120478.
3. J. H. Li, F. Xie, D. Wang, C. Ma, M. Wu, K. Gong, *Constr. Build Mater.*, 303 (2020) 124521.
4. F. Xie, J. H. Li, T. Zou, D. Wang, M. Wu, X. Q. Sun, *Constr. Build Mater.*, 308 (2021) 125093.
5. H.-C. Flemming, J. Wingender, The biofilm matrix, *Nat. Rev. Microbiol.*, 8(9) (2010) 623.
6. Y. Huang, D.K. Xu, L.Y. Huang, Y.T. Lou, J.B. Muhadesi, H.C. Qian, E.Z. Zhou, B.J. Wang, X.T. Li, Z. Jiang, S.J. Liu, D.W. Zhang, C.Y. Jiang, *NPJ Biofilms Microbiol.*, 7(1) (2021) 13.
7. Y.X. Fan, C.Y. Chen, Y.X. Zhang, H.X. Liu, H.W. Liu, H.F. Liu, *Bioelectrochemistry* 141 (2021) 11.
8. H.W. Liu, Y.F. Cheng, *Corros. Sci.*, 173 (2020) 108753.
9. W.W. Dou, J.L. Liu, W.Z. Cai, D. Wang, R. Jia, S.G. Chen, T.Y. Gu, *Corros. Sci.*, 150 (2019) 258.
10. L. Yin, D.K. Xu, C.G. Yang, T. Xi, X.B. Chen, K. Yang, *Corros. Sci.*, 179 (2021) 109141.
11. Z.Y. Li, W.W. Chang, T.Y. Cui, D.K. Xu, D.W. Zhang, Y.T. Lou, H.C. Qian, H. Song, A. Mol, F.H. Cao, T.Y. Gu, X.G. Li, *Commun. Mater.*, 2 (2021) 67.
12. H.W. Liu, Y.X. Zhang, W.H. Li, G.Z. Meng, W. Zhang, H.F. Liu, *Ind. Eng. Chem. Res.*, 58(38) (2019) 17668.
13. H.W. Liu, D.K. Xu, B.J. Zheng, M. Asif, F.P. Xiong, G.A. Zhang, H.F. Liu, *Acta Metall. Sin.*, 31(5) (2018) 456.
14. R. Sueptitz, K. Tschulik, M. Uhlemann, L. Schultz, A. Gebert, *Corros. Sci.*, 53(10) (2011) 3222.
15. B. Guo, P. Zhang, Y. Jin, S. Cheng, *Rare. Metals*. 27(3) (2008) 324.
16. Hong-di, Zhang, Ziao-yu, Jing, Pang, Li-juan, Hai-jian, Ying-jie, Wei-min, Wang, *Int. J. Min. Met. Mater.*, 21(10) (2014) 1009.
17. R. Sueptitz, K. Tschulik, M. Uhlemann, J. Eckert, A. Gebert, *Mater. Corrosion*, 65(8) (2015) 803.
18. R. Sueptitz, K. Tschulik, M. Uhlemann, A. Gebert, L. Schultz, *Electrochim. Acta*. 55(18) (2010) 5200.
19. I. Costa, M.C.L. Oliveira, H.G.D. Melo, R.N. Faria, *J. Magn. Mater.*, 278(3) (2004) 348.
20. M.E. Ghabashy, G.H. Sedahmed, I.A.S. Mansour, *Brit. Corros. J.*, 17(1) (2013) 36.
21. S.L. Zhao, Z.F. You, X.W. Zhang, J.X. Li, *Mater. Charact.*, 174 (2021) 110994.
22. S.L. Zhao, J.J. Bai, Z.F. You, J.X. Li, *Corros. Sci.*, 167 (2020) 108539.
23. H.W. Liu, T.Y. Gu, G.A. Zhang, Y.F. Cheng, H.T. Wang, H.F. Liu, *Corros. Sci.*, 102 (2016) 93.
24. D.X. Sun, M. Wu, F. Xie, *Mat. Sci. Eng. A-Struct.*, 721 (2018) 135.
25. H. Y. Wang, M. Wu, F. Xie, D. Wang, *Journal of Liaoning Shihua University*, 36(04) (2016) 29.
26. B.J. Zheng, K.J. Li, H.F. Liu, T.Y. Gu, *Ind. Eng. Chem. Res.*, 53(1) (2014) 48.
27. W. Haiyan, W. Ming, X. Fei, W. Dan, R. Shuai, G. Xiangshuai, *Journal of Materials Protection*, 49(07) (2016) 9.
28. J. Hu, C.F. Dong, X.G. Li, K. Xiao, *J. Mater. Sci. Technol.*, 26(4) (2010) 355.
29. G. Hinds, J. Coey, M.E.G. Lyons, *Electrochem. Commun.*, 3(5) (2001) 215.
30. S. Legeai, M. Chatelut, O. Vittori, J.P. Chopart, O. Aaboubi, *Electrochim. Acta.*, 50(1) (2005) 51.
31. Z. Lu, C. Huang, D. Huang, W. Yang, *Corros. Sci.*, 48(10) (2006) 3049.

32. R. Sueptitz, K. Tschulik, M. Uhlemann, L. Schultz, A. Gebert, *Corros. Sci.*, 53(10) (2011), 3222.
33. H. Liu, L. Huang, Z. Huang, J. Zheng, *Mater. Corrosion*, 58(1) (2015) 44.
34. Y.J. Li, B. An, Y.G. Wang, Y. Liu, H.D. Zhang, X.G. Yang, W.M. Wang, *J. Non-Cryst. Solids.*, 392-393(7) (2014), 51.
35. R. Sueptitz, K. Tschulik, M. Uhlemann, A. Gebert, L. Schultz, *Electrochim. Acta*, 55 (2010) 5200.

© 2021 The Authors. Published by ESG ([www.electrochemsci.org](http://www.electrochemsci.org)). This article is an open access article distributed under the terms and conditions of the Creative Commons Attribution license (<http://creativecommons.org/licenses/by/4.0/>).